Bending stress and dissipation in subducted lithosphere

B. A. Buffett[1] and T. W. Becker[2]

Received 7 February 2012; revised 9 April 2012; accepted 17 April 2012; published 30 May 2012.

[1] Oceanic lithosphere undergoes permanent deformation during subduction once the stresses exceed the elastic limit. Departures from elastic behavior occur by brittle failure in the shallow lithosphere and by a combination of low- and high-temperature creep at greater depths. We combine laboratory-based rheological models with estimates of slab shape from earthquake hypocenters to quantify the bending stress and dissipation in subduction zones. The peak stress occurs at the depth of the brittle-ductile transition, which is controlled mainly by lithospheric age. Integrals of the stress over the thickness of the plate are used to evaluate the resistive bending force and the bending moment. A representative value for the resistive force on old oceanic lithosphere is 3×10^{12} N m^{-1}, which is comparable in magnitude to ridge push but opposite in direction. Both the bending force and moment are remarkably insensitive to the rate of subduction. In fact, the bending moment can be approximated using a simple power law rheology and a stress exponent of $n \approx 14$. Such a large exponent implies that the lithosphere behaves like a perfectly plastic solid. For most subduction zones the bending moment saturates along the entire plate. As a consequence, the bending stress does not influence the development of curvature during subduction. This behavior may explain why the curvature of subducted lithosphere is nearly independent of age.

Citation: Buffett, B. A., and T. W. Becker (2012), Bending stress and dissipation in subducted lithosphere, *J. Geophys. Res.*, *117*, B05413, doi:10.1029/2012JB009205.

1. Introduction

[2] Subduction of oceanic lithosphere is a fundamental part of plate tectonics. Recycling cold lithosphere into the interior provides an important source of buoyancy for mantle convection [*Richter*, 1973], yet the strength of the lithosphere may impede convection by resisting deformation at the trench [*Conrad and Hager*, 1999; *Becker et al.*, 1999; *Korenaga*, 2003]. Any impediment to motion can be quantified in terms of the work required to bend the lithosphere. Estimates depend on both the stress and the strain rate in the lithosphere. Strain rates can be inferred from changes in the shape of the lithosphere [e.g., *Bevis*, 1986] and Kostrov summation [e.g., *Bevis*, 1988], whereas the stress can be computed with a suitable rheological model. A realistic model is liable to include several types of rheological behavior, depending on the local temperature, pressure and strain rate. Deformation is accommodated by brittle failure in the shallow part of the lithosphere, where the temperature is low and the confining pressure is modest. Ductile deformation (creep) is expected at higher confining pressure, although the mode of deformation is sensitive to temperature. A distinction is made between high- and low-temperature creep to reflect the relative importance of dislocation climb [*Frost and Ashby*, 1982].

[3] Laboratory experiments provide a quantitative description of lithospheric deformation. Studies of frictional sliding suggest that failure on pre-existing faults is well described by a Mohr-Coulomb criterion [*Byerlee*, 1978]. The condition for failure is mainly controlled by the normal stress on the fault with little dependence on temperature or rock type. By contrast, creep is sensitive to both temperature and rock type; most experiments use olivine aggregates to characterize the lithosphere and upper mantle [e.g., *Hirth and Kohlstedt*, 2003]. Rheological models for high-temperature [*Hirth and Kohlstedt*, 2003] and low-temperature [*Mei et al.*, 2010] creep now cover a large span of conditions expected in subducting lithosphere. Consequently, we can combine these rheological models to assess the validity of viscous [*Schellart*, 2009], pseudo-plastic [*Rose and Korenaga*, 2011] and perfectly plastic [*Buffett and Heuret*, 2011] approximations, commonly used in geodynamic models of subduction. Given the large stresses and lower temperatures, it suffices to confine our attention to brittle failure and dislocation creep [*Billen and Hirth*, 2007].

[4] In this study we construct a composite rheology for oceanic lithosphere using Byerlee's law together with laboratory-based models for high- and low-temperature creep in olivine. A kinematic description of strain due to

[1]Department of Earth and Planetary Science, University of California, Berkeley, California, USA.
[2]Department of Earth Sciences, University of Southern California, Los Angeles, California, USA.

Corresponding author: B. A. Buffett, Department of Earth and Planetary Science, University of California, Berkeley, CA 94720, USA. (bbuffett@berkeley.edu)

0148-0227/12/2012JB009205

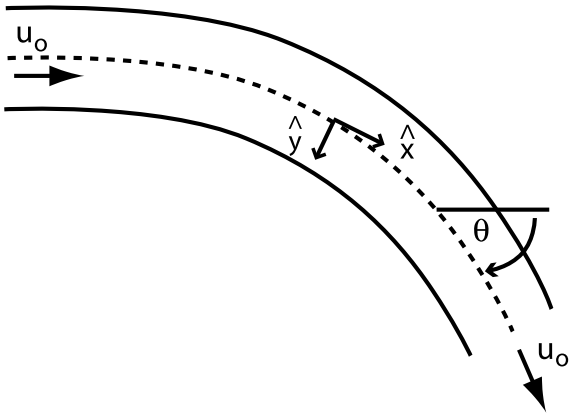

Figure 1. Schematic illustration of subducted lithosphere. Deformation due to bending is described in a coordinate system (x, y, z) that follows the mid-plane of the lithosphere (denoted by dashed line); x is the distance along the mid-plane, y is the distance from the mid-plane and z is perpendicular to the $x - y$ plane. The local dip of the lithosphere is $\theta(x)$ and the curvature $K(x)$ is defined by $K(x) = d\theta/dx$. When there is no strain of the mid-plane (pure bending), the velocity of the mid-plane, u_0, is constant.

bending is used to estimate both the stress and the bending dissipation during subduction. We also introduce a simple power law rheology to approximate the composite rheology. A high stress exponent for the best-fitting power law model suggests that the oceanic lithosphere deforms like a plastic solid during subduction. An important consequence is that the bending stresses do not contribute to the moment balance on the lithosphere; the weight of the slab exerts a torque on the plate, but the response of the lithosphere is largely controlled by stresses on the surface of the plate. Thus the intrinsic strength of the lithosphere does not govern the development of curvature once the elastic limit is exceeded. This result is opposite to expectations for a viscous plate [*Bellahsen et al.*, 2005], but it does explain why the curvature of subducted lithosphere is independent of thickness or age [*Buffett and Heuret*, 2011].

2. Stress and Strain Rate

[5] The geometry of subducted lithosphere is illustrated schematically in Figure 1. Bending at the onset of subduction causes extension above the mid-plane of the plate and compression below. We describe this deformation using a coordinate system that follows the mid-plane of the plate. Let x be the distance along the plate, y be the distance from the mid-plane (positive down), and z be the mutually perpendicular direction (positive into the page). The curvature of the plate, $K(x, t)$, is defined in terms of the local dip angle, $\theta(x, t)$, by $K(x, t) = \partial\theta/\partial x$. When there is no extensional strain along the mid-plane (i.e., pure bending), the strain rate, $\dot{\epsilon}_{xx}$, is given by

$$\dot{\epsilon}_{xx} = -y\frac{DK}{Dt} = -y\left(\frac{\partial K}{\partial t} + u_0\frac{\partial K}{\partial x}\right), \tag{1}$$

where D/Dt denotes the material derivative following the subducted lithosphere and u_0 is the velocity of the mid-plane in the x direction. It is convenient to define the velocity u_0 relative to the position of the trench, so that $\partial K/\partial t$ describes the change in the shape of the subducted plate (or slab) when viewed from the frame of the trench. If the shape of the slab relative to the trench is unchanged during rollback or advance, then $\partial K/\partial t$ vanishes and all of the deformation is due to motion of the slab through the subduction zone at velocity u_0 (sometimes called the subduction velocity). On the other hand, a velocity perpendicular to the mid-plane contributes to both $\partial K/\partial t$ and the deformation.

[6] A combination of numerical models and observations suggest that most of the deformation is due to motion of the slab through the subduction zone. An estimate of curvature along the slab can be inferred from earthquake locations on the slab surface or interior [e.g., *Bevis*, 1986]. A compilation of estimates from the major subduction zones [*Buffett and Heuret*, 2011] suggests that $K(x)$ increases from the trench to the point of maximum curvature (or minimum radius of curvature $R_{\min}$), over a distance that is comparable to $R_{\min}$. Unbending also occurs over a distance of roughly $R_{\min}$ as the slab straightens and descends into the mantle. It follows that the change in curvature along the slab is approximately $\partial K/\partial x \approx \pm R_{\min}^{-2}$, where the sign depends on whether the slab is bending or unbending.

[7] By comparison, $\partial K/\partial t$ is caused by variations in the dip angle with time. A change in dip at the location where the slab straightens ($x \approx 2R_{\min}$) must produce a change in dip throughout the bending/unbending region, although the amplitude of this change decreases toward the trench and vanishes at the surface where the plate is nominally horizontal. From the definition of curvature, we approximate the time dependence using

$$\frac{\partial K}{\partial t} = \frac{\partial}{\partial t}\left(\frac{\partial \theta}{\partial x}\right) = \frac{\partial}{\partial x}\left(\frac{\partial \theta}{\partial t}\right) \approx \frac{1}{L}\left(\frac{\partial \theta(L,t)}{\partial t}\right), \tag{2}$$

where $L \approx 2R_{\min}$ refers to the location where the slab straightens. Numerical models of subduction suggest that the dip at intermediate depths (200 to 400 km) can change by 15 to 20 degrees over 50 million years [*Billen*, 2008], although somewhat larger changes are reported during the transient initiation of subduction. Taking $\partial\theta(L, t)/\partial t = 0.4$ degree/Myr as a plausible estimate for the time dependence, and letting $R_{\min} = 200$ km and $u_0 = 60$ mm/yr, we find that the temporal change in K accounts for about 10% of the deformation. When the dip decreases with time (as observed in the numerical models) the time dependence in K decreases the deformation during bending and increases the deformation during unbending. The opposite occurs when the dip increases with time. In either case the contribution of time dependence to the total dissipation is reduced by the cancelation during bending and unbending. As a result, it suffices to approximate the strain rate using

$$\dot{\epsilon}_{xx} = -yu_0K', \tag{3}$$

where the prime denotes differentiation with respect to x. We take $\dot{\epsilon}_{zz} = 0$ and require $\dot{\epsilon}_{yy} = -\dot{\epsilon}_{xx}$ in an incompressible material.

3. Rheological Models

[8] Stress in the lithosphere is evaluated using the imposed (depth-dependent) strain rate in the rheological models. In

the brittle region we assume that rocks fail by sliding along localized fractures. The shear stress, τ, needed to overcome friction on a surface with normal stress, σ_n, is [*Byerlee*, 1978]

$$\tau = 0.85\,\sigma_n \qquad \text{for } \sigma_n < 200\,\text{MPa}, \tag{4}$$

$$\tau = 50 + 0.6\,\sigma_n \qquad \text{for } \sigma_n > 200\,\text{MPa}. \tag{5}$$

[9] Failure is expressed in terms of the differential (bending) stress, σ_d, using geometric relationships between the failure envelope and principal components of stress. In particular, the slope of the failure envelope determines the orientation of the failure plane relative the direction of the principal stresses. During bending the largest compressive stress is vertical ($\sigma_3 = P$) and the least compressive stress ($\sigma_1 = P - \sigma_d$) represents the direction of tension. Solving for τ and σ_n at failure, and substituting the result into Byerlee's law yields

$$\sigma_d \geq 0.78P \qquad \text{for } \sigma_n < 200\,\text{MPa}, \tag{6}$$

$$\sigma_d \geq 56.6 + 0.68P \qquad \text{for } \sigma_n > 200\,\text{MPa}. \tag{7}$$

[10] In adopting the lower bounds as our estimate for stress in the brittle regime, we assume that fractures have favorable orientation and that the fault strength is not reduced by elevated pore fluid pressure [*Gerya et al.*, 2008].

[11] Stresses in the ductile part of the lithosphere are governed by flow laws for high- and low-temperature creep. The strain rate, $\dot{\epsilon}$, for high-temperature creep is usually represented in the form of a power law

$$\dot{\epsilon} = A_h(\sigma_d)^n \exp\left(-\frac{E(P)}{RT}\right), \tag{8}$$

where σ_d is the differential stress (tension or compression), $n \approx 3.5$ is the stress exponent, $E(P)$ is the pressure-dependent activation energy, T is absolute temperature, R is the gas constant and A_h is a coefficient that can include the influences of water content and melt fraction. Parameter values are taken from *Hirth and Kohlstedt* [2003] for a 'wet' olivine ($A_h = 3.58 \times 10^5$ MPa$^{-3.5}$ s^{-1}, $E(P) = 502$ kJ mol^{-1} at $P = 2$ GPa and a nominal water concentration of 1000 H/10^6 Si). We also consider the rheology for high-temperature creep in dry olivine to assess the possible role of water ($A_h = 1.1 \times 10^5$ MPa$^{-3.5}$ s^{-1} and $E(P) = 550$ kJ mol^{-1} at $P = 2$ GPa).

[12] A different representation is used for low-temperature creep to explicitly account for the stress required to move dislocations (sometimes called the Peierls stress σ_p). The study of *Mei et al.* [2010] expressed the strain rate in the form

$$\dot{\epsilon} = A_l(\sigma_d)^2 \exp\left[-\frac{E(0)}{RT}\left(1 - \sqrt{\frac{\sigma_d}{\sigma_p}}\right)\right], \tag{9}$$

where $E(0) = 320$ kJ mol^{-1} is the activation energy at zero stress, $A_l = 1.4 \times 10^{-7}$ MPa^{-2} s^{-1} is a model constant and the Peierls stress is $\sigma_p = 5.9$ GPa; the exponential dependence on σ_d gives a highly nonlinear flow law.

[13] We do not explicitly consider the elasticity of the plate because the typical curvature during subduction produces elastic stresses that vastly exceed the stresses predicted with either brittle or ductile deformation. Only the innermost 1 or 2 km of the plate is liable to retain its elastic strength, and this region makes only a small contribution to the bending moment and the dissipation. Complete loss of elastic strength is also supported by analysis of gravity-topography admittances [*Billen and Gurnis*, 2005]. Consequently, we use the brittle and ductile rheologies with an imposed strain rate $\dot{\epsilon} = \dot{\epsilon}_{xx}$ to evaluate the stress everywhere in the plate. In the ductile region a combination of low- and high-temperature creep operate in parallel, so we find a single value for the stress $\sigma_d = \sigma_{xx}$ in the sum of (8) and (9) that reproduces the imposed strain rate. Note that the imposed strain rate varies with depth according to (3). For illustrative purposes we evaluate $\dot{\epsilon}_{xx}$ using $u_0 = 60$ mm/yr and $K' = 2.5 \times 10^{-11}$ m^{-2}, but consider a broad range of values in later sections. In addition the stress is strongly dependent on temperature, which we evaluate using a conductive geotherm with a seafloor temperature of 275 K and a mantle temperature of 1600 K. Pressure increases hydrostatically with depth, based on a mean density of 3300 kg m^{-3} and constant gravity $g = 9.8$ m s^{-2}.

[14] Stresses from the brittle and ductile models are evaluated across the entire plate, but the value that is realized at any depth is defined by the minimum stress from either mechanism. A transition from brittle failure to creep occurs at the depth where these two mechanisms give comparable stresses. This transition also coincides with the maximum stress because brittle failure occurs at lower stress when the depth is shallower and ductile stress is reduced by the effects of temperature at greater depths. The transition depth also defines the location of the mid-plane, which ensures that the smallest strain rates occur where the plate is strongest. Because the stress in the ductile region depends on $\dot{\epsilon}_{xx}$, we iteratively adjust an initial estimate for the mid-plane depth until the mid-plane coincides with the peak stress. In detail, the maximum ductile stress occurs a few kilometers below the mid-plane because the strain rate (and hence ductile stress) vanish on the mid-plane. Convergence is achieved once the brittle stress matches the ductile stress a few kilometers below the mid-plane.

[15] Representative examples of the bending stress are shown in Figure 2, specifically for the model that includes high-temperature creep based on wet olivine. Both the mid-plane depth and the maximum stress vary systematically with the age of the lithosphere. Virtually no change in the mid-plane depth or the maximum stress occurs when we adopt the model constants for dry olivine because nearly all of the strain rate in the vicinity of the mid-plane is accommodated by either low-temperature creep or brittle failure. High-temperature creep is only effective in the lower part of the plate, where the temperature is sufficiently high. The onset of high-temperature creep can be detected as a slight change in the slope of the stress versus depth in the region below the mid-plane. The choice of dry olivine causes a small increase in the stress near the base of the plate (relative to that shown in Figure 2) and produces a modest 10% increase in the bending moment (see below). This difference is small relative to other uncertainties. The depths and focal mechanisms of outer-rise earthquakes limit the mid-plane depth to roughly 25 to 40 km [*Chapple and Forsyth*, 1979; *Forsyth*, 1982]. Agreement with the results in Figure 2 lend

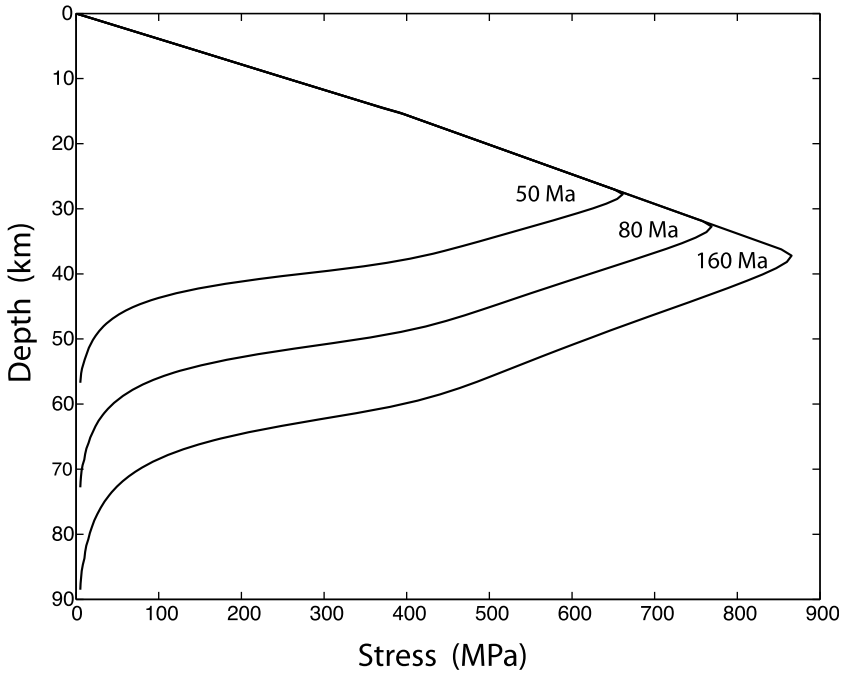

Figure 2. Stress in the lithosphere due to bending at a subduction zone. The maximum stress coincides with a transition between brittle failure (above) and creep (below). A conductive geotherm defines the temperature through the lithosphere. Calculations for lithospheric ages of 50, 80 and 160 Ma yield progressively thicker and stronger lithosphere. Constant values for the plate velocity and the rate of change of curvature are assumed in the calculations (see text), but other choices have only a weak influence on the stress state.

support to the rheological models for brittle failure and low-temperature creep.

4. Mechanical Properties of Subducted Lithosphere

[16] Several physical quantities can be computed from the stress profiles in Figure 2. For instance, the mechanical thickness of the lithosphere can be defined by the region where the strength of the lithosphere exceeds some threshold (say a few MPa). Alternatively, we could define the mechanical thickness as twice mid-plane depth because the stress is nearly symmetric about the mid-plane. Both definitions give roughly similar results. On the basis of the mid-plane depth we obtain a mechanical thickness of $H_m = 56$, 66 and 76 km for lithospheric ages 50, 80 and 160 Ma. These values are roughly 50% to 60% of the thermal thickness $H_T = 2.32\sqrt{\kappa t}$ [e.g., *Parsons and Sclater*, 1977], where $\kappa = 10^{-6}$ m^{2}s^{-1} is the thermal diffusivity and t is the age. (By this definition the thermal lithosphere represents 90% of the total temperature change across the thermal boundary layer.)

[17] Another quantity of interest is the bending moment

$$M(x) = \int_{-H_m/2}^{H_m/2} y\,\sigma_{xx}\,dy, \tag{10}$$

where the limits of integration depends on the mechanical thickness H_m. Both the stress, σ_{xx}, and thickness, H_m, are calculated using the rheological models for a given plate age, curvature and velocity. The integral for $M(x)$ is obtained numerically using Simpson's rule. Figure 3 shows how $M(x)$ varies over a broad range of values for the plate velocity. For a given age (or thickness) the bending moment is relatively

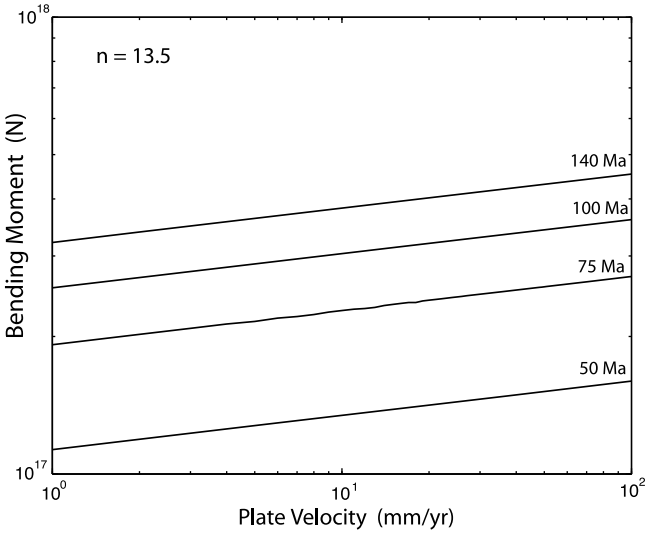

Figure 3. The bending moment, $M(x)$, as a function of the plate velocity for several ages (50, 75 100 and 140 Ma). Weak variations in $M(x)$ with u_0 are consistent with the predictions of a power law model. The best-fitting slope corresponds to a stress exponent of $n = 13.5$.

insensitive to changes in the plate velocity. Such a weak dependence of $M(x)$ on velocity (or strain rate) is diagnostic of plastic materials. (A more quantitative assessment is given below.) For the limiting case of perfect plasticity we expect the bending moment to saturate during subduction. Once $M(x)$ saturates the largest subsequent change in the moment occurs at the point of maximum curvature, where the plate begins to unbend. At that point the sign of K' changes and the sense of strain reverses from tension to compression (or vice versa on the other side of the mid-plane). After the moment changes sign, a new level of saturation is established.

[18] The moment during unbending is not constrained by the stress state during bending. Brittle failure under compression occurs at larger differential stress compared with failure under tension [e.g., *McNutt and Menard*, 1982]. A higher confining pressure may further enhance the brittle strength of the lithosphere as the plate subducts to greater depths. On the other hand, the ductile stress may decrease once the plate begins to warm. For the purpose of estimating the dissipation we make the simple assumption that the moment during unbending is equal in magnitude to the moment during bending.The rate of dissipation per unit length of plate is

$$\phi(x) = \int_{-H_m/2}^{H_m/2} \dot{\epsilon}_{xx}\,\sigma_{xx}\,dy = -u_0 K' M(x), \tag{11}$$

where $\dot{\epsilon}_{xx}$ is defined in (3). The strain rate $\dot{\epsilon}_{yy} = -\dot{\epsilon}_{xx}$ does not contribute to $\phi(x)$ because we make the usual assumption that the non-hydrostatic stress σ_{yy} vanishes in a thin plate. Note that the dissipation is always positive because K' and $M(x)$ have opposite sign. Integrating $\phi(x)$ over the length of the plate gives the total dissipation

$$\Phi = -u_0 M_{sat} \int |K'| dx, \tag{12}$$

where $|\cdot|$ denotes the absolute value and M_{sat} is the saturated (constant) value of $M(x)$ during bending; by assumption the moment during unbending is $M(x) = -M_{sat}$. For a simple subduction zone where K' changes sign only once at the point of maximum curvature (denoted by $K_{\max}$), we can replace $\int |K'| dx$ in (12) with $2K_{\max}$. This approximation is used below to quantify the influence of bending on the dynamics of subduction.

[19] Bending produces a net horizontal force on the plate at the trench. *Buffett* [2006] showed that the force due to bending can be expressed as $F_b = -\Phi/u_0$. It follows that the bending dissipation is equal to the work done against the resistive bending force. Using the approximation $\Phi = -2u_0 K_{\max} M_{sat}$ gives $F_b = 2K_{\max} M_{sat}$. Taking $M_{sat} = -4.5 \times 10^{17}$ N-m/m as a representative value for old oceanic lithosphere and $K_{\max} = 6.7 \times 10^{-6}$ m^{-1} as an average value for the Japan-Kurile subduction zone [*Buffett and Heuret*, 2011], we obtain $F_b = -3 \times 10^{12}$ N m^{-1}. (The negative sign indicates that this force opposes the motion of the plate.) This force is comparable in magnitude to ridge push and about a factor of ten smaller than slab pull [*Turcotte and Schubert*, 1971], although much of the weight of the slab is probably supported by shear stresses on the surface of the descending plate. Numerical simulations of subduction suggest that the stress transmitted through the plate to the surface produces a net force of 6.5×10^{12} N m^{-1} or less [*Capitanio et al.*, 2009]. Since this force has been reduced by F_b through the zone of bending (and unbending), the net force below the bend might be as large as 9.5×10^{12} N m^{-1}. Thus effects of bending could reduce the in-plate force by 30% or more. On the other hand, the work done against F_b is about 10% of the total work done by slabs sinking through the upper mantle. A few subduction zones in the western Pacific have maximum curvature that exceeds the average value for the Japan-Kuriles, but the largest bending dissipation is unlikely to exceed 20% of the total work due to slab pull.

[20] *Di Giuseppe et al.* [2008] predicted a larger bending dissipation (30–50%), based on numerical calculations with an effective viscosity that is roughly a thousand times larger than the upper mantle value. *Wu et al.* [2008] adopted a similar viscosity but obtained a lower dissipation by using a smaller average curvature during subduction. The lower dissipation in the study of *Wu et al.* [2008] gave better agreement with the speed of observed of plate motions. However, the dissipation in a viscous plate depends on $(K')^2$, integrated along the entire length of the slab [*Buffett*, 2006]. The exact integral for dissipation in a thin viscous sheet can be approximated in terms of the maximum curvature (rather than the average curvature), although other approximations have been proposed [*Ribe*, 2010]. Making this change in the study of *Wu et al.* [2008] substantially increases the dissipation. A lower dissipation can be achieved with a plastic rheology [*Buffett and Heuret*, 2011], although the peak value reported in that study (less than 40%) is probably too high because the thermal thickness H_T was used to approximate H_m.

5. A Simple Power Law Rheology

[21] The weak dependence of the bending moment on the plate velocity suggests that the lithosphere as a whole behaves like a plastic solid during subduction. We quantify this suggestion by showing that a simple power law model with a high stress exponent can be used to approximate the laboratory-based rheology. The power law model is constructed using the Levy-Mises equation [*Hill*, 1964]

$$\dot{\epsilon}_{ij} = \frac{1}{2\eta}\left(\sigma_{II}^{n-1}\right)\sigma'_{ij}, \tag{13}$$

where η is a material constant, σ'_{ij} are the deviatoric components of the stress tensor and $\sigma_{II} = \sqrt{J_2}$ is defined in terms of the second invariant $J_2 = \sigma'_{ij}\sigma'_{ij}/2$. Noting that the second invariant of the strain rate tensor is

$$D_2 = \frac{1}{2}\dot{\epsilon}_{ij}\dot{\epsilon}_{ij} = \dot{\epsilon}_{xx}^2. \tag{14}$$

We find from (13) that

$$\dot{\epsilon}_{xx}^2 = \frac{1}{4\eta^2}\sigma_{II}^{2n}. \tag{15}$$

Consequently, the deviatoric components of stress are

$$\sigma'_{xx} = 2\eta(2\eta|\dot{\epsilon}_{xx}|)^{-(n-1)/n}\dot{\epsilon}_{xx}, \tag{16}$$

$$\sigma'_{yy} = -2\eta(2\eta|\dot{\epsilon}_{xx}|)^{-(n-1)/n}\dot{\epsilon}_{xx}. \tag{17}$$

The total stress (deviatoric plus mean stress $\bar{\sigma}$) is

$$\sigma_{xx} = \bar{\sigma} + \sigma'_{xx}, \tag{18}$$

$$\sigma_{yy} = \bar{\sigma} + \sigma'_{yy}, \tag{19}$$

which implies that $\bar{\sigma} = -\sigma'_{yy}$ because $\sigma_{yy} = 0$. Substituting the mean stress into (18) gives the desired result for the bending stress

$$\sigma_{xx} = 2s(2\eta|\dot{\epsilon}_{xx}|)^{1/n}, \tag{20}$$

where s denotes the sign of $\dot{\epsilon}_{xx}$ (e.g., $s = 1$ for $\dot{\epsilon}_{xx} > 0$). Integrating σ_{xx} for the bending moment $M(x)$ yields

$$M(x) = -\frac{n}{2n+1}(\eta u_0 K')^{1/n} H_m^{(2n+1)/n}, \tag{21}$$

when $K' > 0$ and

$$M(x) = \frac{n}{2n+1}(\eta u_0 K')^{1/n} H_m^{(2n+1)/n}, \tag{22}$$

when $K' < 0$.

[22] Limiting cases for $M(x)$ correspond to viscous and perfectly plastic rheologies. The usual result for a viscous plate emerges when $n = 1$ [e.g., *De Bremaecker*, 1977]. In this case the material constant, η, corresponds to the plate viscosity. The bending moment (and force) has a linear dependence on the plate velocity and a strong H_m^3 dependence on the mechanical thickness. As a result the bending force increases more rapidly with age than the force due to slab pull, which depends linearly on the thermal thickness $H_T \approx 2H_m$. A perfectly plastic behavior occurs when $n \to \infty$. In this case the bending moment (and force) is independent of u_0 and varies with mechanical thickness as H_m^2 [e.g., *Turcotte et al.*, 1978]. Once again the bending force increases more rapidly with age than slab pull. Consequently, the bending force exerts the greatest resistance on old oceanic lithosphere, which can lead to preferential subduction of lithosphere with intermediate age [*Buffett and Rowley*, 2006; *Becker et al.*, 2009].

[23] An effective stress exponent for the composite, laboratory-based, rheology can be inferred from the weak dependence of $M(x)$ on u_0 in Figure 3. The best-fitting slope of $M(x)$ versus u_0 gives $M \propto u_0^{0.074}$ with little variability about this fit. In other words, a single value for the exponent in the power law model does a very good job in approximating the moment computed using the laboratory-based rheology. According to (21) and (22), the laboratory-based rheology is well described with a stress exponent of $n = 13.5$. This value is large enough to approximate the perfectly plastic limit. In the plastic limit the bending dissipation is proportional to u_0^1 [*Buffett*, 2006], whereas the laboratory-based rheology gives $u_0^{1.07}$. A weak velocity dependence has also been obtained in numerical calculations of *Rose and Korenaga* [2011], which combined a pseudo-plastic rheology with high-temperature creep above a critical temperature. Their estimate of the bending dissipation was roughly proportional to $u_0^{1.2}$. The weaker velocity dependence in the present study is probably due to our treatment of low-temperature creep.

6. Forces on Subducted Lithosphere

[24] A plastic rheology has a number of consequences for the force balance on subducted lithosphere. For example the saturation of the bending moment affects the development of curvature through the subduction zone. Evidence for saturation at the trench was previously noted by *Goetze and Evans* [1979], based on observations of lithospheric flexure. In addition, the deflection of slabs at the 670-km discontinuity has been used to argue for plastic deformation [*Cizkova et al.*, 2002]. Here we use the power law rheology from the previous section to evaluate the bending moment along the entire length of subducted lithosphere. This calculation requires an estimate for the plate curvature, which can be determined using the location of hypocenters in a subduction zone. Two-dimensional profiles were defined by *Heuret and Lallemand* [2005] for all of the major subduction zones, and hypocenters within approximately 100 km of each profile were compiled by *Heuret* [2005] using locations from *Engdahl et al.* [1998]. A spline fit through the hypocenters defines a smooth surface for computing the curvature [*Buffett and Heuret*, 2011]. To illustrate the saturation of the bending moment, we consider a profile from the central Aleutians (identified as CALE5 in *Wu et al.* [2008]). The plate age and velocity at the trench from *Wu et al.* [2008] are 58 Ma and 61.4 mm/yr, respectively.

[25] Figure 4 shows the spline fit through earthquake locations for profile CALE5. The curvature, $K(x)$, is computed from the local dip of the smooth surface in Figure 4a. The distance along the mid-plane, x, originates at the start of the spline fit on the seaward side of the trench and continues until the seismicity terminates at depth. Curvature increases over the first 200 km and steadily decreases over the next 200 km. In this simple (but typical) example, K' changes sign only once at the point of maximum curvature.

[26] A reference value for the moment is calculated using the laboratory-based rheology and a nominal value for K' (denoted by K'_{ref}). The moment for other values of K' can be extrapolated using the power law model to give

$$M(K') = \pm M\left(K'_{ref}\right)\left(\frac{K'}{K'_{ref}}\right)^{1/n}, \tag{23}$$

where $M(K'_{ref}) = -1.8 \times 10^{17}$ N m is evaluated using $K'_{ref} = 5 \times 10^{-6}$ m^{-1}. (The plate velocity and age are treated as constants). A stress exponent of $n = 13.5$ is chosen to approximate the results of the laboratory-based rheology, while the sign of M depends on the sign of K', according to (21) and (22). The derivative, $K'(x) = dK/dx$, is computed from the spline fit. Substituting $K'(x)$ into (23) determines the moment as a function of distance along the mid-plane (see Figure 5).

[27] Variations in the bending moment are relatively small during the initial increase in curvature, indicating that the bending moment is effectively saturated. A more abrupt change in $M(x)$ occurs at the point of maximum curvature,

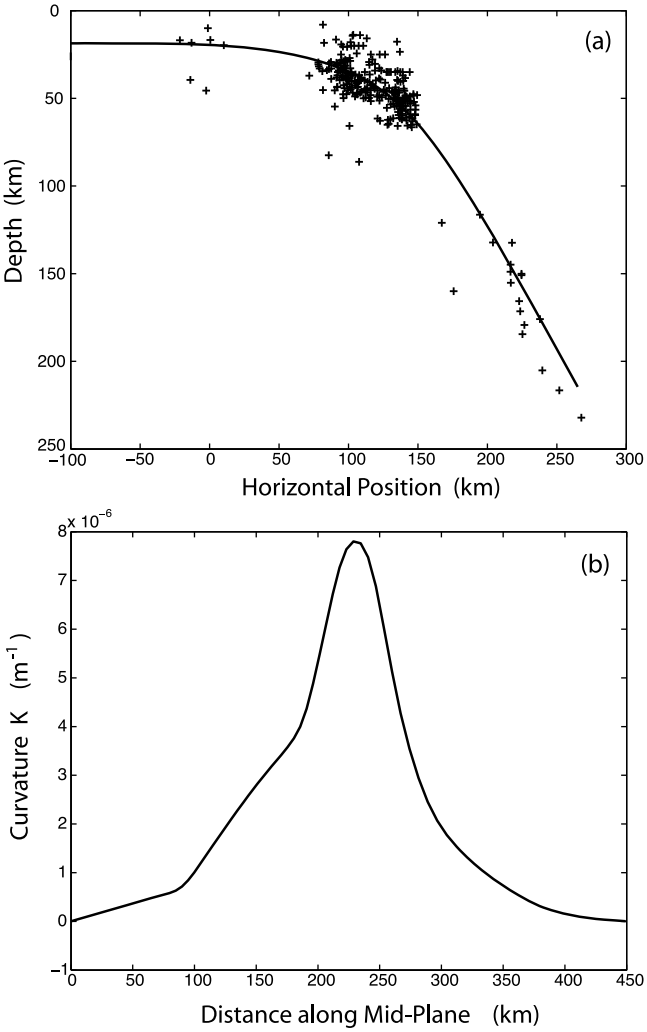

Figure 4. Two-dimensional profile of subducted lithosphere from earthquake locations in the central Aleutians. (a) A smooth spline is fit through the hypocenters (crosses) to approximate the mid-plane of the plate. The horizontal position is defined relative to the trench. (b) The curvature of the lithosphere is calculated as a function of distance, x, along the slab. The origin $x = 0$ refers to the starting position of the spline fit on the seaward side of the trench.

where K' changes sign. During unbending the moment saturates at roughly the same magnitude because the simple power law rheology makes no distinction between bending and unbending. The derivative, $M' = dM/dx$, is strongly peaked at the location of maximum curvature, but nearly vanishes elsewhere (see Figure 5b). The observation that M' vanishes away from the point of maximum curvature has important consequences for the torque balance on the plate.

[28] For illustration we consider the force and torque balance on the plate when the forces on the top and bottom surfaces are small (see Figure 6). Such an approximation is appropriate when the plate is strong compared with the surrounding mantle. The leading-order balance of forces in the direction perpendicular to the plate is

$$\frac{dQ}{dx} + H_m \Delta\rho(\mathbf{g}\cdot\hat{\mathbf{y}}) \approx 0, \tag{24}$$

where $H_m \Delta\rho(\mathbf{g}\cdot\hat{\mathbf{y}})$ is the $\hat{\mathbf{y}}$ component of the buoyancy force due to the excess density of the plate and Q is the net force due to shear stresses in the plate,

$$Q = \int_{-H_m/2}^{H_m/2} \sigma_{xy}\, dy. \tag{25}$$

[29] The key point is that buoyancy produces shear stresses in the plate when there are no other forces on the top or bottom surfaces.

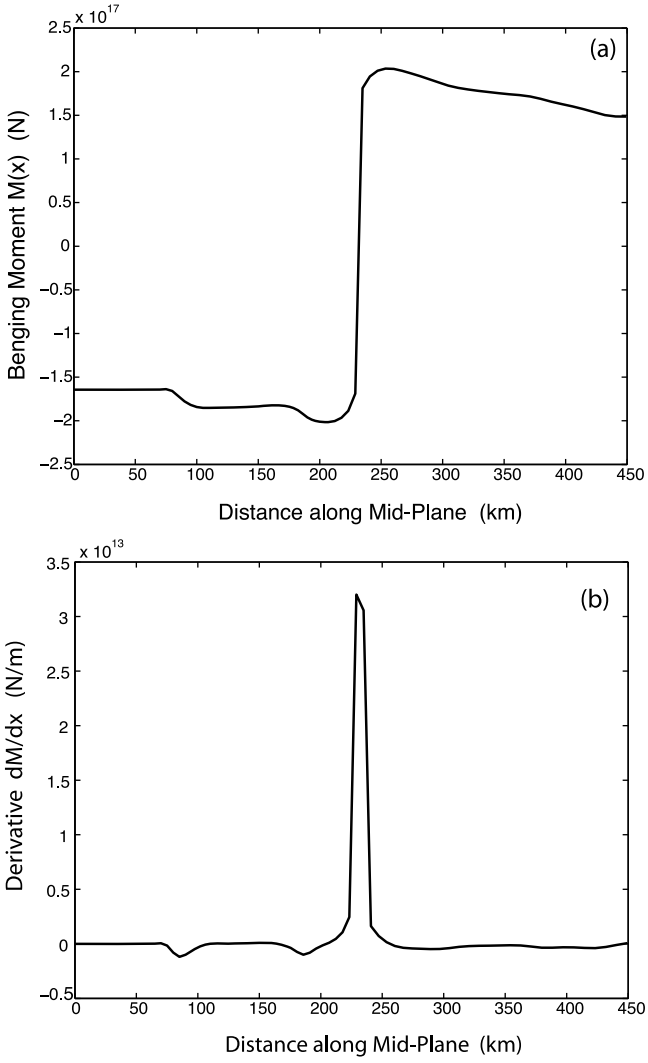

Figure 5. Bending moment along a slab in the central Aleutians, based on the power law rheology with a stress exponent of $n = 13.5$. Both the stress exponent and the material constant, η, are chosen to reproduce the results of the laboratory-based rheology (see text). (a) The bending moment is nearly constant as the curvature increases ($K' > 0$), consistent with expectations that the moment saturates during subduction. Once the plate begins to straighten ($K' < 0$) the bending moment changes sign and adjusts to a new value, which is comparable in magnitude to the moment during bending. (b) The derivative dM/dx is strongly peaked at the location where K' switches sign. In the limit of a perfectly plastic material the moment is approximated by a step function and the derivative can be represented by a delta function.

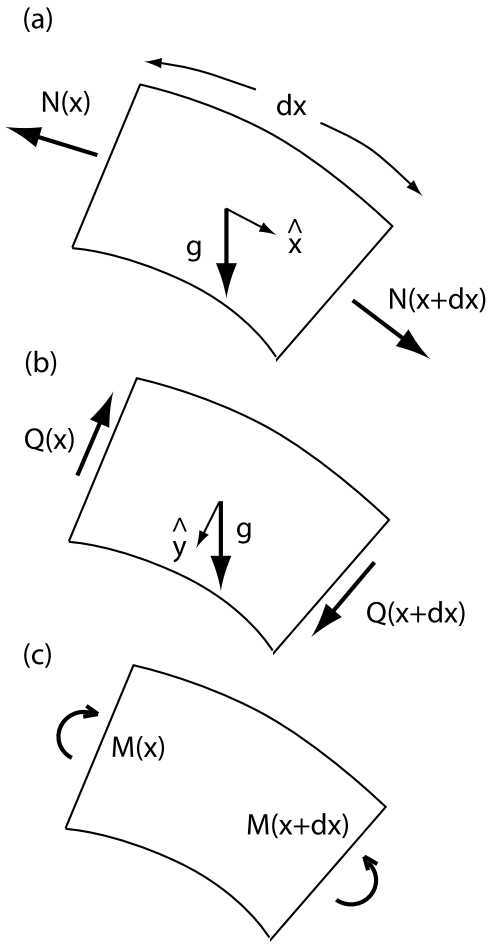

Figure 6. Schematic illustration of the forces and torques associated with internal stresses and buoyancy in a short segment of subducted lithosphere. Not shown are the additional contributions due to the effects of curvature or due to forces on the top and bottom surfaces of the plate. (a) Forces in the plane of the plate include the $\hat{\mathbf{x}}$ component of the buoyancy force and the net force, N, due to normal stresses σ_{xx}. (b) Forces perpendicular to the plate include the $\hat{\mathbf{y}}$ component of the buoyancy force and the net force, Q, due to shear stresses σ_{xy}. (c) A torque balance in the absence of forces on the top and bottom of the plate includes contributions from the shear force Q and the bending moment M.

[30] Figure 6b shows that shear stresses also contribute to the torque balance on a plate. We maintain a balance by opposing the torque due to Q with the bending moment M. The leading-order description of the torque balance is

$$M' \approx Q, \tag{26}$$

which poses a problem when the bending moment saturates because $M' = 0$. This means that the torque balance cannot be achieved without additional forces. One way to enforce the torque balance is to apply a differential pressure across the plate. If the differential pressure is large enough to balance the buoyancy force in Figure 6b, then Q would vanish and the torque balance would reduce to $M' \approx Q \approx 0$. The required differential pressure might develop as a result of low pressure in a thin, lubricating layer on top of the plate [e.g., *Leal*, 2007]. Alternatively, the pressure difference might also arise due to the effects of corner flow [*Stevenson and Turner*, 1977; *Tovish et al.*, 1978].

[31] A second way to enforce the torque balance in a plastic plate is to apply shear stresses to the top and bottom of the plate. However, we cannot simply rely on shear stresses due to relative motion of the plate because to the torque depends on differences between the shear stress on the top and bottom surfaces. A large shear stress on the interface with the overriding plate might yield the required torque, although it is doubtful that this stress is sufficient to achieve a torque balance, assuming that the magnitude of the shear stress is comparable to a typical stress drop during intraplate earthquakes [*Kanamori and Anderson*, 1975].

[32] It is useful to compare the plastic rheology with the behavior of a viscous plate. Using (24) to eliminate Q from the torque balance gives

$$\frac{d^2M}{dx^2} = -H_m \Delta\rho(\mathbf{g} \cdot \hat{\mathbf{y}}). \tag{27}$$

[33] In effect, the buoyancy force exerts a torque on the plate, which is balanced by bending stresses inside the plate. Substituting for M from (21) and (22) gives

$$\frac{d^3K}{dx^3} = \frac{3\Delta\rho(\mathbf{g} \cdot \hat{\mathbf{y}})}{\eta u_0 H_m^2}, \tag{28}$$

which describes the development of curvature along the plate during subduction. Buoyancy drives an increase in curvature, whereas the viscosity, η, and thickness, H_m, of the plate oppose the increase in curvature. In fact, the local dip, θ, of the plate is governed by

$$\frac{d^4\theta}{dx^4} = \left(\frac{3\Delta\rho g}{\eta u_0 H_m^2}\right)\cos\theta, \tag{29}$$

where g is the magnitude of the gravity vector $\mathbf{g}$. We conclude that the curvature of a highly viscous plate should depend on both viscosity and thickness, whereas the distribution of earthquake hypocenters in subduction zones suggests that the curvature of the lithosphere is independent of thickness [*Buffett and Heuret*, 2011]. This insensitivity to thickness is entirely consistent with a plastic rheology. Because the moment saturates during subduction, bending stresses cannot balance the torque arising from buoyancy. The inherent strength of the plate, as defined by the bending moment, has no role in the evolution of curvature. This result appears to be consistent with observations.

[34] A plastic rheology also has relevance for the transmission of stresses through the plate to the surface. Because the rheology is weakly dependent on strain rate, the strength of the plate under uniform tension should not be very different from the strength associated with bending. In fact, the stress in the brittle region should be identical because the stress state is tensional in both cases. Compression occurs below the mid-plane during bending, but low-temperature

creep has no explicit dependence on the sign of differential stress. Consequently, the strength of the lithosphere in the ductile region should be similar in compression and tension. Integrating the stress σ_{xx} across the thickness of the plate, e.g.,

$$N = \int_{-H_m/2}^{H_m/2} \sigma_{xx}\, dy \tag{30}$$

defines the force transmitted through the plate. Using the stresses from Figure 2 to evaluate N gives an upper bound. For plate ages $t = 50$, 80 and 160 Ma, we obtain $N_{\max} = 1.7 \times 10^{13}$, 2.5×10^{13} and 3.4×10^{13} N m^{-1}, which are all above the values usually reported in numerical simulations of subduction [*Capitanio et al.*, 2009]. This suggests that the strength of the plate is not a limiting factor in transmitting stress to the surface. While failure is expected near the surface of the plate, a strong central region near the mid-plane allows for effective transmission of stress. Numerical calculations that include a high-viscosity core [e.g., *Capitanio et al.*, 2009; *Stegman et al.*, 2010] should reproduce this effect. Equal care is needed to quantify the resistance due to to bending.

[35] The bending force in a viscous plate can be approximated by [*Buffett*, 2006]

$$F_b = -\frac{2}{3}\eta u_0 H_m^3 K_{\max}^3, \tag{31}$$

where $K_{\max}$ is the maximum curvature. By comparison, the bending force for the composite rheology was approximated by

$$F_b = 2K_{\max} M_{sat}, \tag{32}$$

which means that the effective viscosity of the plate (particularly the outer parts of the plate) should be chosen to satisfy

$$M_{sat} \approx -\frac{1}{3} H_m^3 K_{\max}^2 \eta u_0. \tag{33}$$

[36] Taking $M_{sat} = -4.5 \times 10^{17}$ N and $H_m = 80$ km for old oceanic lithosphere, together with $u_0 = 60$ mm/yr and $K_{\max} = 5 \times 10^{-6}$ m^{-1}, gives $\eta = 5.5 \times 10^{22}$ Pa s. On the other hand, it might be preferable to avoid a velocity-dependent viscosity by using a power law rheology with a large stress exponent [e.g., *Krien and Fleitout*, 2008].

[37] To conclude we show that the bending force for the composite rheology emerges in a straightforward way from the in-plane force balance on the lithosphere (Figure 6a). When there are no surface forces on the plate, the equation for the force balance in the $\hat{\mathbf{x}}$ direction reduces to [*Ribe*, 2001]

$$\frac{dN}{dx} - K\frac{dM}{dx} = -H_m(\mathbf{g}\cdot\hat{\mathbf{x}})\Delta\rho\left(1 + \frac{K^2 H_m^2}{12}\right), \tag{34}$$

where $\mathbf{g}$ is the acceleration due to gravity and $\Delta\rho$ is the excess density of the plate relative to the mantle. Allowing for surface forces adds more terms to (34), but it does not alter the calculation of the bending force. Integrating (34) over the length of the plate from $x = 0$ to $x = L$ gives

$$N(0) = N(L) - \int_0^L K\frac{dM}{dx}\, dx + \int_0^L H_m(\mathbf{g}\cdot\hat{\mathbf{x}})\Delta\rho\left(1 + \frac{K^2 H_m^2}{12}\right) dx. \tag{35}$$

[38] Thus the horizontal force on the plate at the surface, $N(0)$, has three contributions in (35). The last term represents the weight of the slab (i.e., slab pull), whereas the second term represents the resistive bending force. The first term defines the stress state at depth, which can be eliminated from (35) by choosing L to coincide with the depth where stress in the plate changes from tension ($N > 0$) to compression ($N < 0$) [*Isacks and Molnar*, 1971]. Noting that dM/dx vanishes over most of the plate, the bending force can be written as

$$F_b = -\int_0^L K\frac{dM}{dx}\, dx = 2K_{\max} M_{sat}, \tag{36}$$

which is identical to the estimate of the force based on bending dissipation. If the sign of K' changed several times over the length of the plate, multiple peaks in dM/dx would be expected. To calculate F_b we would need to sum these individual contributions or (equivalently) replace $2K_{\max}$ with $\int |K'|dx$. The bending force abruptly alters $N(x)$ at locations where K' changes sign. In most cases this coincides with the maximum curvature of the plate. An abrupt drop in $N(x)$ might be reflected in a change in the orientation of focal mechanisms above and below the point of maximum curvature because the background stress state should be altered, particularly in old oceanic lithosphere.

7. Conclusions

[39] Laboratory-based rheological models are used to determine the strength of oceanic lithosphere during subduction. Estimates of stress are obtained with an imposed kinematic description of the strain rate to define the mechanical thickness of the lithosphere, which is typically 50% to 60% of the thermal thickness. The stresses also determine the moment, force and dissipation associated with bending at subduction zones. The bending moment is weakly dependent on velocity, indicating a nearly plastic behavior. A simple power law model is developed to quantify the degree of plasticity. The best-fitting slope of the bending moment versus the plate velocity corresponds to a power law model with a stress exponent of $n = 13.5$.

[40] One consequence of a large stress exponent is that the bending moment saturates during subduction. Stresses associated with bending in a plastic plate cannot balance the torque associated with buoyancy forces. Instead, surface forces on the plate must play an important role. Consequently, the conditions in the overriding plate should contribute, and possibly control, to the evolution of curvature. The bending force in old oceanic lithosphere is approximately 3×10^{12} N m^{-1}, based on a representative estimate for slab curvature. The corresponding dissipation is about 10% of the work done by slabs sinking through the upper mantle, although a few subduction zones with larger

curvature can dissipate as much as 20%. Further insights into the dynamics of subduction might be sought in the focal mechanisms of subduction earthquakes. An abrupt change in the normal force $N(x)$ is expected when the plate switches between bending and unbending. Such a change in the background stress state might be reflected in the orientation of focal mechanisms.

[41] **Acknowledgments.** This work is partially supported by a collaborative research grant from the National Science Foundation (EAR-0911255). We thank two anonymous reviewers for many constructive comments and suggestions.

References

Becker, T. W., C. Faccenna, R. J. O'Connell, and D. Giardini (1999), The development of slabs in the upper mantle: Insights from numerical and laboratory experiments, *J. Geophys. Res.*, *104*, 15,207–15,225.

Becker, T. W., C. P. Conrad, B. A. Buffett, and R. D. Mueller (2009), Past and present seafloor age distributions and the temporal evolution of plate tectonic heat transport, *Earth Planet. Sci. Lett.*, *278*, 233–242.

Bellahsen, N., C. Faccenna, and F. Funicello (2005), Dynamics of subduction and plate motion in laboratory experiments: Insights into the plate tectonics behavior of the Earth, *J. Geophys. Res.*, *110*, B01401, doi:10.1029/2004JB002999.

Bevis, M. (1986), The curvature of Wadati-Benioff zones and the torsional rigidity of subducting plates, *Nature*, *323*, 52–53.

Bevis, M. (1988), Seismic slip and down dip strain rate in Wadati-Benioff zones, *Science*, *240*, 1317–1319, doi:10.1126/science.240.4857.1317.

Billen, M. I. (2008), Modeling the dynamics of subducting slabs, *Ann. Rev. Earth Planet. Sci.*, *36*, 325–356.

Billen, M. I., and M. Gurnis (2005), Constraints on subducting plate strength within the Kermadec trench, *J. Geophys. Res.*, *110*, B05407, doi:10.1029/2004JB003308.

Billen, M. I., and G. Hirth (2007), Rheologic controls on slab dynamics, *Geochem. Geophys. Geosyst.*, *8*, Q08012, doi:10.1029/2007GC001597.

Buffett, B. A. (2006), Plate force due to bending at subduction zones, *J. Geophys. Res.*, *111*, B09405, doi:10.1029/2006JB004295.

Buffett, B. A., and A. Heuret (2011), Curvature of subducted lithosphere from earthquake locations in the Wadati-Benioff zone, *Geochem. Geophys. Geosyst.*, *12*, Q06010, doi:10.1029/2011GC003570.

Buffett, B. A., and D. B. Rowley (2006), Plate bending at subduction zones: Consequences for the direction of plate motions, *Earth Planet. Sci. Lett.*, *245*, 359–364.

Byerlee, J. D. (1978), Friction of rocks, *Pure Appl. Geophys.*, *116*, 615–626.

Capitanio, F. A., G. Morra, and S. Goes (2009), Dynamics of plate bending at the trench and slab-plate coupling, *Geochem. Geophys. Geosyst.*, *10*, Q04002, doi:10.1029/2008GC002348.

Chapple, W. M., and D. W. Forsyth (1979), Earthquakes and bending of plates at trenches, *J. Geophys. Res.*, *84*, 6729–6749.

Cizkova, H., J. van Hunen, A. P. van den Berg, and N. J. Vlaar (2002), The influence of rheological weakening and yield stress on the interaction of slabs with the 670-km discontinuity, *Earth Planet. Sci. Lett.*, *119*, 447–457.

Conrad, C. P., and B. H. Hager (1999), The effects of plate bending and fault strength at subduction zone on plate dynamics, *J. Geophys. Res.*, *104*, 17,551–17,571.

De Bremaecker, J. C. (1977), Is the oceanic lithosphere elastic or viscous?, *J. Geophys. Res.*, *82*, 2001–2004.

Di Giuseppe, E., J. van Hunen, F. Funiciello, C. Faccenna, and D. Giaardini (2008), Slab stiffness control of trench motion: Insights from numerical models, *Geochem. Geophys. Geosyst.*, *9*, Q02014, doi: 10.1029/2007GC001776.

Engdahl, R. E., R. van der Hilst, and R. Burland (1998), Global teleseismic earthquake relocation with improved travel times and procedures for depth determination, *Bull. Seismol. Soc. Am.*, *88*, 722–743.

Forsyth, D. W. (1982), Determination of focal depths of earthquakes associated with the bending of oceanic plates at trenches, *Phys. Earth Planet. Inter.*, *28*, 141–160.

Frost, H. J., and M. F. Ashby (1982), *Deformation Mechanism Maps*, 167 pp., Pergamon, New York.

Gerya, T. V., J. A. D. Connolly, and D. A. Yuen (2008), Why is terrestrial subduction one-sided?, *Geology*, *36*, 43–46.

Goetze, C., and B. Evans (1979), Stress and temperature in bending lithosphere as constrained by experimental rock mechanics, *Geophys. J. R. Astron. Soc.*, *59*, 463–478.

Heuret, A. (2005), Dynamique des zone de subduction: Etude statistique globale et approache anologique, Ph.D. thesis, Univ. Montpellier II, Montpellier, France.

Heuret, A., and S. Lallemand (2005), Plate motions, slab dynamics and back-arc deformation, *Phys. Earth Planet. Inter.*, *149*, 31–51.

Hill, R. (1964), *The Mathematical Theory of Plasticity*, 355 pp., Oxford Univ. Press, New York.

Hirth, G., and D. L. Kohlstedt (2003), Rheology of the upper mantle and mantle wedge: A view from the experimentalists, in *Inside the Subduction Factory*, *Geophys. Monogr. Ser.*, vol. 138, edited by J. Eiler, pp. 83–105, AGU, Washington, D. C., doi:10.1029/138GM06.

Isacks, B., and P. Molnar (1971), Distribution of stress in descending lithosphere from a global survey of focal-mechanism solutions of mantle earthquakes, *Rev. Geophys.*, *9*, 103–174.

Kanamori, H., and D. L. Anderson (1975), Theoretical basis of some empirical relationships in seismology, *Bull. Seismol. Soc. Am.*, *65*, 1073–1095.

Korenaga, J. (2003), Energetics of mantle convection and the fate of fossil heat, *Geophys. Res. Lett.*, *30*(8), 1437, doi:10.1029/2003GL016982.

Krien, Y., and L. Fleitout (2008), Gravity above subduction zones and forces controlling plate motions, *J. Geophys. Res.*, *113*, B09407, doi: 10.1029/2007JB005270.

Leal, L. G. (2007), *Advanced Transport Phenomena: Fluid Mechanics and Convective Transport*, 912 pp., Cambridge Univ. Press, New York.

McNutt, M. K., and H. W. Menard (1982), Constraints on yield strength in the oceanic lithosphere derived from observations of flexure, *Geophys. J. R. Astron. Soc.*, *71*, 363–394.

Mei, S., A. M. Suzuki, D. L. Kohlstedt, N. A. Dixon, and W. B. Durham (2010), Experimental constraints on the strength of lithospheric mantle, *J. Geophys. Res.*, *115*, B08204, doi:10.1029/2009JB006873.

Parsons, B., and J. G. Sclater, (1977), Analysis of variation of ocean-floor bathymetry and heat flow with age, *J. Geophys. Res.*, *82*, 803–827.

Ribe, N. M. (2001), Bending and stretching of thin viscous sheets, *J. Fluid Mech.*, *433*, 135–160.

Ribe, N. M. (2010), Bending mechanics and mode selection in free subduction: A thin-sheet analysis, *Geophys. J. Int.*, *180*, 559–576.

Richter, F. M. (1973), Dynamic models for sea-floor spreading, *Rev. Geophys.*, *11*, 223–287.

Rose, I. R., and J. Korenaga (2011), Mantle rheology and the scaling fo bending dissipation in plate tectonics, *J. Geophys. Res.*, *116*, B06404, doi:10.1029/2010JB008004.

Schellart, W. P. (2009), Evolution of the slab bending radius and the bending dissipation in three-dimensional subduction models with a variable slab to upper mantle viscosity ratio, *Earth Planet. Sci. Lett.*, *288*, 309–319, doi:10.1016/j.epsl.2009.09.03.

Stegman, D. R., R. Farrington, F. A. Capitanio, and W. P. Schellart (2010), A regime diagram for subduction styles from 3D numerical models of free subduction, *Tectonophysics*, *483*, 29–45.

Stevenson, D. J., and J. S. Turner (1977), Angle of subduction, *Nature*, *270*, 334–336.

Tovish, A., G. Schubert, and B. P. Luyendyk (1978), Mantle flow pressure and the angle of subduction: Non-Newtonian corner flow, *J. Geophys. Res.*, *83*, 5892–5898.

Turcotte, D. L., and G. Schubert (1971), Structure of the olivine-spinel phase boundary in the descending lithosphere, *J. Geophys. Res.*, *76*, 7980–7987.

Turcotte, D. L., D. C. McAdoo, and J. G. Caldwell (1978), An elastic-perfectly plastic analysis of the bending of the lithosphere at a trench, *Tectonophysics*, *47*, 193–205.

Wu, B., C. P. Conrad, A. Heuret, C. Lithgow-Bertelloni, and S. Lallemand (2008), Reconciling strong slab pull and weak plate bending: The plate motion constraint on mantle slabs, *Earth Planet. Sci. Lett.*, *272*, 412–421.